ACS Photonics

Article

pubs.acs.org/journal/apchd5

# Synergetic Effect of Silver Nanocrystals Applied in PbS Colloidal Quantum Dots for High-Performance Infrared Photodetectors

Jungang He,[†,§] Keke Qiao,[‡,§] Liang Gao,[‡] Haisheng Song,*[,‡] Long Hu,[‡] Shenglin Jiang,*[,†] Jie Zhong,[‡] and Jiang Tang*[,‡]

[†]School of Optical and Electronic Information and [‡]Wuhan National Laboratory for Optoelectronics (WNLO), Huazhong University of Science and Technology (HUST), 1037 Luoyu Road, Wuhan, Hubei 430074, People's Republic of China

Supporting Information

**ABSTRACT:** PbS colloidal quantum dot (CQD) photodetectors hold great potential for near-infrared detection due to their extremely high sensitivity and low-cost solution processing. In this paper we report that incorporation of 0.5% to 1% (by weight) Ag nanocrystals (NCs) into the PbS CQDs film could simultaneously enhance the photocurrent and suppress dark current and hence significantly boost device detectivity. A set of control experiments suggested that Ag NCs, once added to the PbS CQD film, could trap photogenerated electrons from neighboring PbS CQDs, extend carrier lifetime, and increase photocurrent. We further built a sensitive flexible photodetector using the optimized composite on stone paper, achieving an estimated detectivity as high as $1.5 \times 10^{10}$ Jones. The synergetic effect found in our PbS CQD/Ag NC composite photodetectors is expected to be extendable to other binary NC systems for various applications.

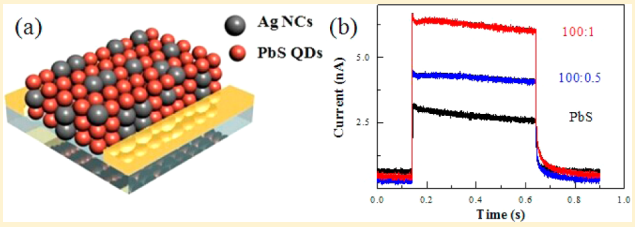


**KEYWORDS:** *PbS colloidal quantum dots, Ag nanocrystals, nanocomposites, photodetectors, flexibility*

Photodetection in the infrared (IR) has a wide range of applications in both commercial and scientific fields including spectroscopy,[1] communications,[2] biomedical imaging,[3] and night vision.[4] Current IR photodetection employs photodetectors made from indium gallium arsenide (InGaAs)[5] and mercury cadmium tellurium (HgCdTe).[6] These photodetectors, although very sensitive and robust, are grown by expensive epitaxy method that are incompatible with flexible polymer substrates because of the lattice matching requirement and high-temperature processing. Therefore, it is highly desirable to develop new IR photodetectors that possess the merit of low cost and mild fabrication conditions.

As a promising alternative, lead sulfide (PbS) colloidal quantum dots (CQDs) have attracted significant research interest for near-IR detection because of their band-gap tunability, which could be utilized to customize the detection range, and also because of their solution processability, which enables these photodetectors to be readily integrated with the complementary metal−oxide−semiconductor platforms and also with flexible substrates.[7,8] Moreover, solution-processed PbS CQD photoconductive photodetectors have achieved ultrahigh detectivity of $\sim 1.8 \times 10^{13}$ Jones working at room temperature,[9,10] exceeding the epitaxy-grown InGaAs photodetectors. Recently, PbS CQD composites were intensively studied for photodetector application, aiming at better device performance from the synergetic effect of hybrid components.[11,12] For example, J. Curry et al. utilized $C_{60}$ fullerite crystal nanowires and a PbS CQD hybrid system to implement broadband photodetectors from near UV to infrared.[13] G. Konstantatos et al. adopted a graphene sheet and PbS CQD system to obtain conductive photodetectors with a gain of up to $10^8$,[14] while the gain for PbS CQDs alone devices only reached $10^2$−$10^3$.[1,9,15] Despite the demonstrated beneficial effects, a PbS CQD-based composite for photodetection is relatively less explored.

For a photoconductive photodetector, detectivity ($D^*$) is the figure of merit to compare the performance of different devices. Detectivity is defined by the responsivity ($R$), device area ($A$), electrical bandwidth ($B$), and noise current ($I_n$) through the equation $D^* = R(Af)^{1/2}/I_n$. Responsivity is defined by the output photocurrent ($I_p$) divided by the incident power ($P$). As for the noise current, noise associated with current fluctuation flowing across a photodetector often dominates the total noise of the detector,[16] so $I_n$ could be approximately correlated with the dark current ($I_d$) following $I_n = (2qI_dB)^{1/2}$, where $q$ is the elementary charge. Consequently, for a photoconductive photodetector with given device area and electrical bandwidth, to engineer the photodetector with maximized photocurrent and minimized dark current would significantly enhance the device detectivity. Unfortunately, it is very challenging to increase photocurrent and suppress dark current simultaneously because these two factors often strongly interact with each other and alter unidirectionally. For example, improvement in carrier mobility increases both photocurrent and dark current, while a decrease in doping density often reduces both

**Received:** February 27, 2014
**Published:** September 12, 2014

  

photocurrent and dark current. To our best knowledge, there is no such report yet on PbS CQD photodetectors where a single process is capable of increasing photocurrent and reducing dark current simultaneously.

In this paper, we report that by introducing Ag nanocrystals (NCs) into a PbS CQD film and building the PbS CQD/Ag NC composite active layer we could improve the photocurrent and suppress the dark current of our photodetectors simultaneously. Specifically, 0.5% and 1% (by weight) Ag NCs were mixed with PbS CQDs in solution, and we then fabricated the photoconductive photodetectors using the well-established layer-by-layer spin-coating procedure.[17] Devices with Ag NC incorporation showed slightly reduced dark current but almost doubled photocurrent, leading to an approximately 3-fold improvement in estimated device detectivity. We then carefully investigated the underlying mechanisms and ruled out possible effects from synthesis impurities or in situ formed $Ag_2S$ species. We thus tentatively ascribed our observation to the trapping of photogenerated electrons by Ag NCs from neighboring PbS CQDs. Furthermore, we also built a composite photodetector with excellent sensitivity and robust flexibility. Our findings provide a valued example of a synergetic effect in binary NC systems for photodetector applications, and this observation may extend to other material systems for various applications.

## RESULTS AND DISCUSSION

We first study the ingredients of our composite for photoconductive photodetectors. PbS CQDs, capped by oleate ligand, were synthesized using the hot injection method first developed by Hines.[18] Ag NCs were prepared by the reduction of $AgNO_3$ in oleylamine.[19] Oleylamine also served as the capping ligand, preventing Ag NCs from precipitation in octane. The absorption spectrum of PbS CQDs (Figure 1a)

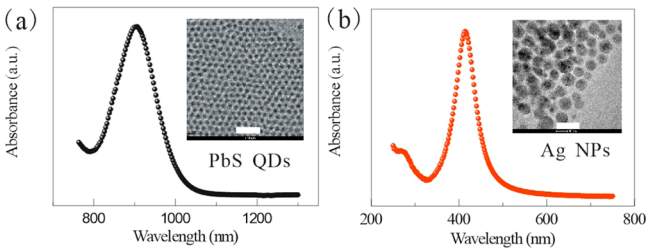


**Figure 1.** Material characterization of the as-synthesized PbS CQDs and Ag NCs: (a) PbS CQDs characterized by UV−vis and TEM (inset). The absorption excitonic peak is located at 902 nm, corresponding to a PbS CQD diameter of ∼3 nm. (b) UV−vis spectrum and TEM image (inset) of pure Ag NCs (∼10 nm). The absorption peak is at 408 nm. The scale bar for both TEM images is 20 nm.

showed an excitonic absorption peak located at 902 nm, which indicated the average size of our PbS CQDs was 3 nm based on the equation proposed by Moreels.[20] The full width at half-maximum (fwhm) of ∼144 nm of the excitonic peak confirmed the small size distribution of our PbS CQD ensemble. This analysis is confirmed by the transmission electron microscopy (TEM) observation shown as an inset in Figure 1a. Ag NCs were also characterized by UV−vis absorption spectrum and TEM (Figure 1b). Ag NCs showed a characteristic plasmonic absorption peak centered at 408 nm, and TEM characterization indicated the average size of the Ag NCs was approximately 10 nm.

Photoconductive photodetectors were fabricated using PbS CQD/Ag NC composites. For device fabrication, PbS CQDs dispersed in octane (50 mg/mL) and Ag NCs dispersed in octane (5 mg/mL) were blended with a given ratio and then magnetically stirred to ensure complete mixing. The weight ratios (PbS CQDs:Ag NCs) explored were 100:0 (no Ag NCs, control), 100:0.5, and 100:1. We then spun the mixed octane solution onto ceramic substrates with prepatterned interdigitated Au electrodes, which have a length of 3 mm and spacing of 0.5 mm. Layer-by-layer spin-coating was adopted to build a PbS CQD/Ag NC composite film with ∼100 nm thickness. 3-Mercaptopropionic acid (MPA) solution (10% v/v in methanol) was applied for the treatment to remove the original insulating oleate ligand and passivate PbS CQD surface defects.[21] The spin-coating process was carried out at room temperature in ambient air. Figure 2a schematically depicts the device configuration of our photoconductive photodetectors: the PbS CQD (small red spheres) and Ag NCs (large gray spheres) composite film was sandwiched between two Au electrodes. PbS CQDs and Ag NCs were believed to randomly scattered within the film (Figure S1), although a small ratio of local aggregation and phase separation was also possible. Device performance was measured using an Agilent B1500A in an optically and electrically shielded probe station. Good ohmic contact was observed for all three samples, as evidenced by the perfect linear current−voltage ($I$−$V$) curves shown in Figure 2b. This is expected because MPA-treated PbS CQD film is moderately p-type doped and forms good ohmic contact with a high work function Au electrode. Furthermore, incorporation of Ag NCs into the PbS CQD film reduced film conductivity, 100:1 composite sample showing the lowest conductivity. This is quite surprising because normally addition of metal NCs improves film conductivity by the formation of a conductive channel within the CQD film[21,22]

The reduced conductivity was also presented in the dynamic current−time ($I$−$t$) curves shown in Figure 2c. For the three PbS CQDs/Ag NCs (100:0, 100:0.5, and 100:1) devices, the dark current and photocurrent were 0.7 and 3.1 nA, 0.3 and 4.4 nA, and 0.4 and 6.5 nA, respectively, when the bias was 40 V and light illumination was 36 $\mu W/cm^2$. Apparently, addition of Ag NCs suppressed dark current and enhanced photocurrent simultaneously, an improvement that is very beneficial for photodetection yet rarely observed before. As a result, the responsivity for the 100:0, 100:0.5, and 100:1 devices was 1.5, 2.5, and 3.8 mA/W, respectively. By assuming the noise of our photodetector was dominated by the shot noise, we estimated the detectivity ($D^*$) to be $2.1 \times 10^{10}$, $5.4 \times 10^{10}$, and $7.1 \times 10^{10}$ Jones, respectively. A full set of device parameters is summarized in Table 1. An incorporation of 1% Ag NCs into the PbS CQD film leads to a 238% net gain in device detectivity, suggesting the synergetic effect between Ag NCs and PbS CQDs. It is noticeable that our photodetectors showed much smaller responsivity than previous reports[23] (on the order of a few hundred A/W). For a photoconductive photodetector illuminated by light with a given wavelength ($\lambda$), device responsivity ($R$) is correlated with the absorption efficiency ($\eta$), trap lifetime ($\tau$), and the majority carrier transit time ($\tau_T$) by the following equation:

$$R = \frac{\eta q \lambda}{hc} G = \frac{\eta q \lambda}{hc} \frac{\tau}{\tau_T} \quad (1)$$


dx.doi.org/10.1021/ph500227u | ACS Photonics 2014, 1, 936−943

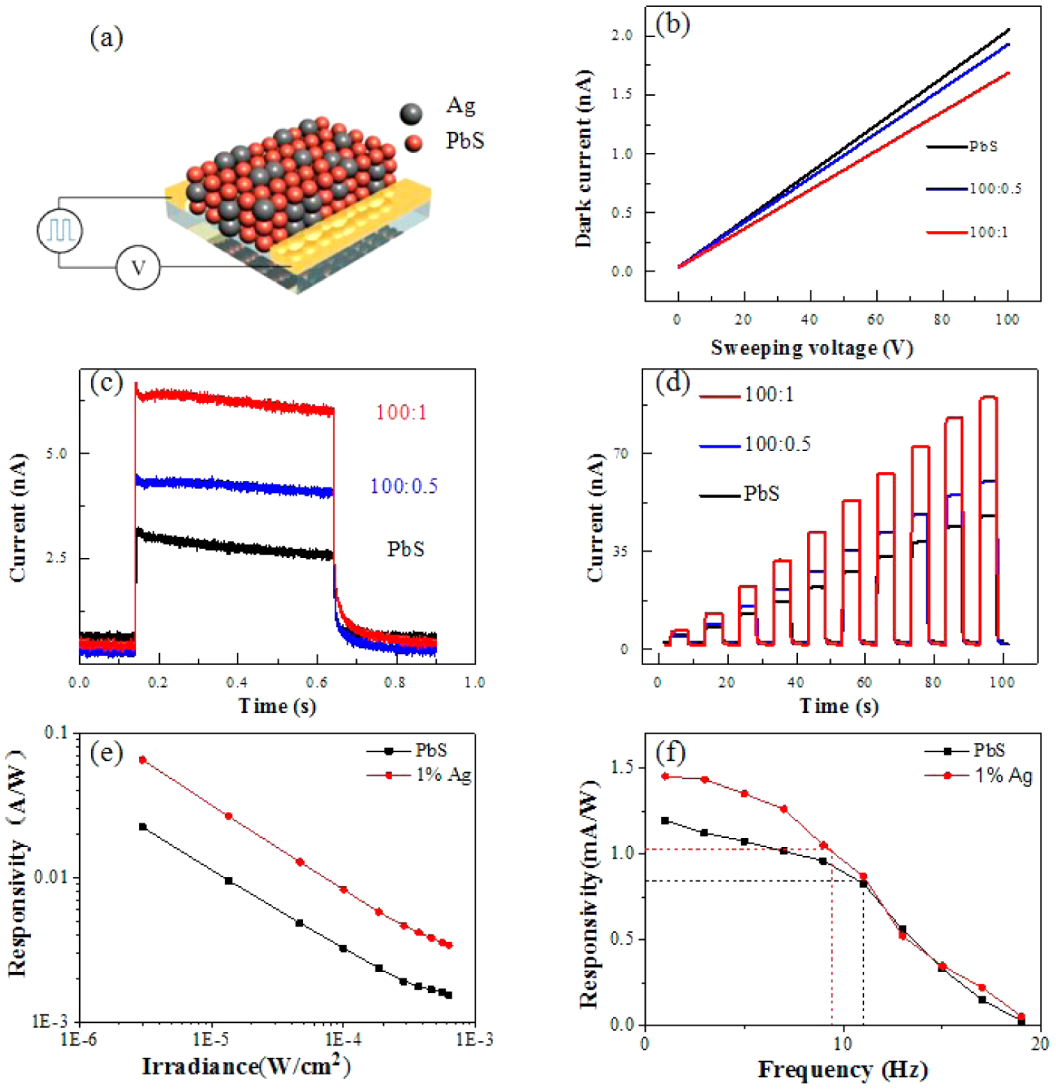


**Figure 2.** Photodetector performances based on PbS CQDs and Ag NC composites. (a) Schematic demonstration of device configuration. Red spheres represent PbS CQDs, and black spheres represent Ag NCs. (b) Dark current–voltage ($I$–$V$) curves of our control and PbS CQD/Ag NC photodetectors. (c) Dynamic current–time ($I$–$t$) curves of PbS CQDs/Ag NC composite (100:0, 100:0.5, and 100:1) photodetectors under 36 $\mu$W/cm$^2$ illumination and 40 V voltage. (d) $I$–$t$ curves of our photodetectors illuminated by pulsed incident light with varied power density from 36 to 1500 $\mu$W/cm$^2$. (e) Irradiance-dependent responsivity of our control and the 1% Ag NC composite device. Illumination intensity varied from $10^{-6}$ to $10^{-3}$ W/cm$^2$ with a bias voltage of 100 V. (e) Frequency dependence of PbS CQD and 1% Ag NC composite photodetector. The dashed line corresponds to 70.7% of the initial value, and hence the 3 dB frequency for the control and 1% Ag NC device was 11.0 and 9.4 Hz, respectively. For all measurements the device area was 0.015 cm$^2$.

**Table 1. Summary of Device Performance for Our Photodetectors Working at 36 $\mu$W/cm$^2$ Illumination and 40 V Voltage in Figure 2c[a]**

| PbS/Ag | $I_d$ (nA) | $I_p$ (nA) | $I_p/I_d$ | responsivity (mA/W) | $D^{**}10^9$ (Jones) |
|---|---|---|---|---|---|
| 100:0 | 0.7 | 3.1 | 4.4 | 1.5 | 21 |
| 100:0.5 | 0.3 | 4.4 | 14.7 | 2.5 | 54 |
| 100:1 | 0.4 | 6.5 | 16.3 | 3.8 | 71 |

[a] $I_d$: dark current; $I_p$: photocurrent; $D^*$: detectivity.

where $q$ is the elementary charge, $h$ is Plank's constant, $c$ is light speed, and $G$ is gain defined as $G = \tau/\tau_T$. The transit time ($\tau_T$) is the time for the holes to travel across the CQD film between the two Au electrodes. Naturally, it is determined by the device geometry and external bias (V):

$$\tau_T = \frac{L^2}{V\mu} \quad (2)$$

where $L$ is the interelectrode spacing and $\mu$ is carrier mobility. Since $L$ is as long as 0.5 mm in our device, while literature values are often 5 $\mu$m, this will result in a $10^4$ times smaller $R$ in our case, providing all other parameters are identical. Such a calculation suggests that the quality of our photodetectors was comparable with that in previous reports.

It should be emphasized that the somewhat unusual improvement by the incorporation of Ag NCs was consistently observed for many devices fabricated by different operators and using different batches of PbS CQDs, ruling out the possibility of experimental artifacts. We also noted that for devices incorporating 2% or even higher Ag NCs, device performance improvement is less reproducible and sometimes even resulted in significantly reduced photocurrent. We thus conclude that


dx.doi.org/10.1021/ph500227u | ACS Photonics 2014, 1, 936–943

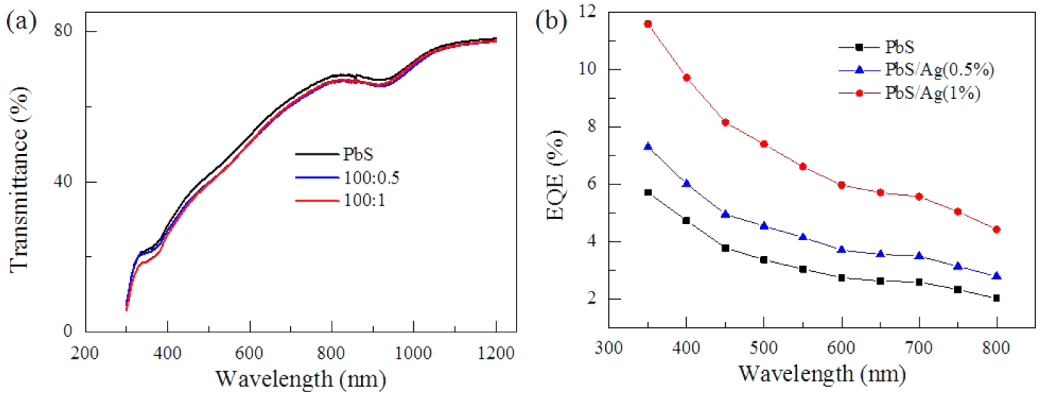


**Figure 3.** (a) Absorption spectra and (b) EQE spectra of our composite photodetector containing 0%, 0.5%, and 1% Ag NCs.

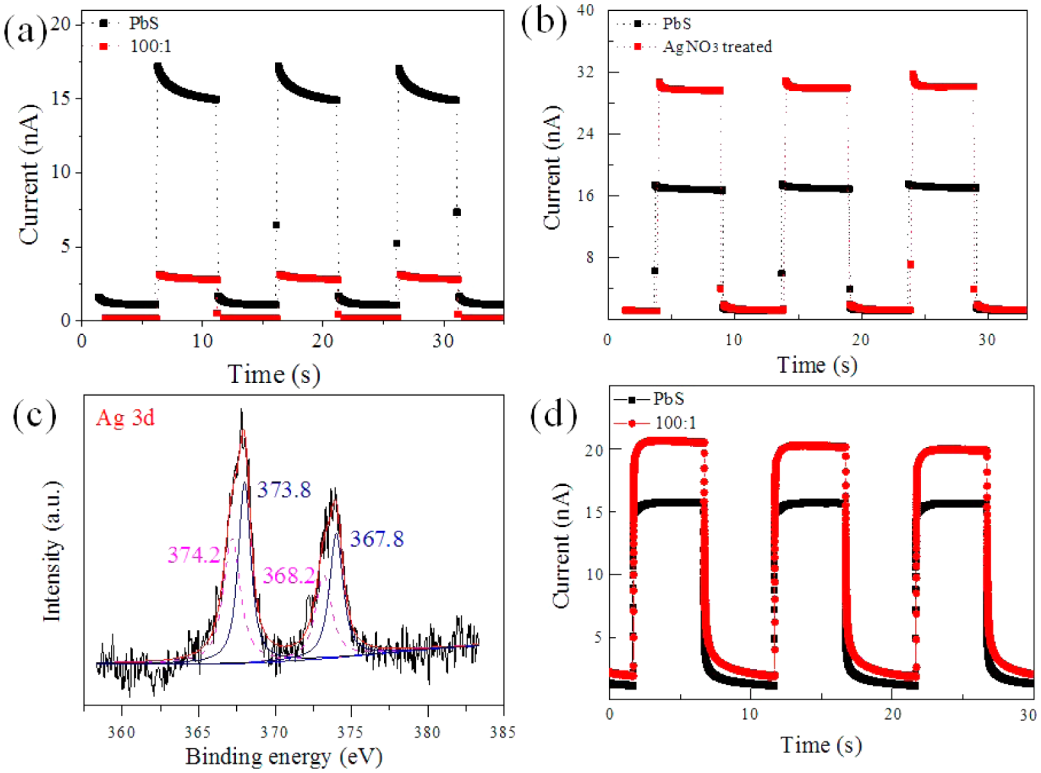


**Figure 4.** Hunting for a smoking gun for the observed photocurrent enhancement and dark current suppression by Ag NC inclusion: (a) *I*–*t* curves of a PbS CQD photodetector with and without 1% oleylamine inclusion. (b) *I*–*t* curves of a PbS CQD photodetector with and without 10 mg/mL $AgNO_3$ methanol solution treatment for 15 s. (c) XPS analysis of the Ag signal in the PbS CQD/Ag NC composite film. Gaussian–Lorentzian fitting was applied to the peaks to identify different chemical state of Ag. (d) *I*–*t* curves of the PbS CQD photodetector with and without inclusion of 1% (by weight) $Ag_2S$ NCs.

1% Ag NC is optimal for the performance of our PbS CQD/Ag NC composite photodetectors.

We further measured the performance of our photodetectors under different light intensities (Figure 2d, from 36 to 1500 $\mu W/cm^2$): photodetectors having Ag NCs all showed enhanced photocurrent and suppressed dark current without exception, as compared to the PbS CQDs alone device. By calculating the device responsivity under different light intensities, we plotted the illumination-dependent responsivity in Figure 2e. Apparently, the *R* value decreased monotonically when the illumination intensified. This is understandable because the gain, and also the responsivity, is tightly related to carrier lifetimes (eqs 1 and 2). At low light intensities, photogenerated electrons would be captured by deep traps, resulting in longer carrier lifetime and hence higher responsivity. At high light intensities, deep traps are filled, and then photogenerated electrons will be captured by shallower ones. Under such circumstances, the average carrier lifetime drops, leading to a reduced responsivity, the so-called dynamic-range enhancing gain compression under increased illumination.[24]

For photodetection, sensing speed is another crucial factor to be considered. We measured the photoresponse of our device under modulated illumination and plotted the result in Figure 2f. The 3 dB frequency, defined as the frequency at which the responsivity declines to 70.7% of its initial value, was measured to be 11.0 Hz for the control device and 9.4 Hz for the 1% Ag NC composite device, respectively. The underlying reason for the reduced photoresponse speed will be discussed later, and


dx.doi.org/10.1021/ph500227u | ACS Photonics 2014, 1, 936–943

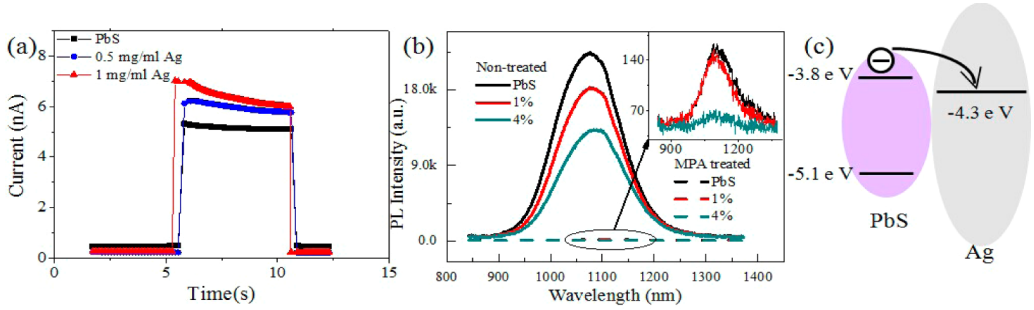


**Figure 5.** (a) Dynamic $I-t$ curves of bilayered photodetectors by spin-coating PbS CQDs on top of a Ag NC layer, which is spun from a 0.5 or 1 mg/mL Ag NC octane solution. (b) PL spectra of PbS CQD/Ag NC composite including different amounts of Ag NCs with and without MPA treatment. (c) Energy levels of PbS CQD and Ag NCs; photogenerated electrons could easily transfer from the CB of PbS to Ag NCs.

further optimization is required to improve the 3 dB frequency to higher values.

We now discuss the origin of our observation. We first check the plasmonic-enhanced light absorption from Ag NCs, since G. Konstantatos's group reported broadband responsivity enhancement in PbS CQD photodetectors by the islandized Ag NC film on a glass substrate produced from thermal evaporation.[11,25,26] As shown in Figure 3a, the absorption spectra of a composite film (PbS CQD:Ag NCs of 100:0, 100:0.5, and 100:1) were measured and compared. The excitonic peaks of PbS CQDs were preserved in the film, but no significant absorption enhancement was observed in the composite film. We further measured the external quantum efficiency (EQE) of our photodetectors. For the composite device, the EQE spectrum showed a universal and smooth increase from 300 to 800 nm as compared to the control device and no abrupt gain at ~410 nm. The plasmonic absorption peak of our Ag NCs was observed for devices containing 0.5% and 1% Ag NCs. Both the optical absorption and EQE results excluded that photocurrent enhancement originated from plasmonic enhancement of light absorption derived from Ag NCs.

Another possibility is the impurities contained in the Ag NC solution. Our Ag NCs were synthesized using $AgNO_3$ as the precursor and oleylamine as the solvent and capping ligands, and these two chemicals could be the leftovers coexisting in the Ag NC solution. We thus studied the effect of oleylamine and $AgNO_3$ on the performance of PbS CQD photodetectors. To do this, we intentionally add 1% (by weight) oleylamine to the PbS CQD solution and fabricated devices using the identical procedures to those stated before. Device performance is shown in Figure 4a. The addition of 1% oleylamine resulted in significantly reduced photocurrent and dark current: the control device showed an $I_d$ and $I_p$ of 1.1 nA and 15.3 nA, respectively, while the 1% oleylamine device showed an $I_d$ of 0.4 nA and an $I_p$ of 3.1 nA. Similarly, we also included $AgNO_3$ in PbS CQD photodetectors by immersing the device into a $AgNO_3$ methanol solution for 15 s. For the $AgNO_3$-treated device, the photocurrent improved from 17.2 nA to 29.9 nA and the dark current also increased from 1.2 nA to 1.4 nA (Figure 4b), a simultaneous enhancement of both photocurrent and dark current. Clearly, neither oleylamine nor $AgNO_3$ is responsible for the observed simultaneous dark current suppression and photocurrent enhancement.

It is also possible that new species formed in situ in the PbS CQD/Ag NC composite that accounted for the simultaneously increased photocurrent and reduced dark current. X-ray diffraction (XRD) characterization was applied to measure the composite (Figure S2,), and no new species was observed in the XRD patterns other than PbS CQDs and Ag NCs. We then applied X-ray photoemission spectroscopy (XPS) to study our PbS CQD/Ag NC composite. In addition to the strong peaks from lead and sulfur (Figure S3), XPS peaks ascribed to Ag 3d were also detected. Careful analysis of the Ag 3d peaks (Figure 4c) suggested two kinds of chemical species: peaks located at 374.2 and 368.2 eV were identified as silver metal $Ag^0$, while peaks located at 373.8 and 367.8 eV corresponded to silver ions $Ag^+$ in $Ag_2S$ judged by their binding energy.[27] Despite that these $Ag^+$ ions could be the leftover $AgNO_3$ precursor, they most likely originated from the reaction between Ag NCs and MPA leading to the formation of $Ag_2S$ at the surface of Ag NCs. The Tian group utilized a similar reaction to produce carboxylic acid-terminated $Ag_2S$ NCs in a few minutes.[28] In order to study the influence of in situ formed $Ag_2S$ on the photoresponse of our device, $Ag_2S$ NCs were separately synthesized (confirmed by XRD, shown in Figure S4) and blended with PbS CQDs to fabricate photoconductive photodetectors. Figure 4d showed the $I-t$ curves of the control device as well as the device containing 1% (by weight) $Ag_2S$ NCs. Again, both the photocurrent and dark current were increased, in a similar way to the photodetectors treated by $AgNO_3$ but to a lesser extent.

Having excluded the possible contributions from impurities or in situ formed $Ag_2S$, we tentatively ascribe the beneficial effect to the electron-trapping effect of Ag NCs. To confirm this, we built a bilayer device by spin-coating MPA-treated PbS CQDs on top of Ag NCs. A Ag NC octane solution of 0.5 and 1 mg/mL was spun once, most likely producing a discontinuous Ag NC film. PbS CQDs were then spun on top, finishing the bilayer device. For the control device, $I_d$ is 0.5 nA and $I_p$ is 5.3 nA, while for the device having one layer of Ag NCs (spun from 0.5 mg/mL), $I_d$ is 0.2 nA and $I_p$ is 6.2 nA (Figure 5a). Obviously, the underneath Ag NC layer significantly improved the photocurrent and reduced the dark current, just like the PbS CQD/Ag NC composite device. We also blended PbS CQDs with Ag NCs and measured their photoluminescence. As shown in Figure 5b, for the composite film with or without MPA treatment, introduction of Ag NCs suppressed the photoluminescence of PbS CQDs, especially for the sample containing 4% Ag NCs. Such a photoluminescence quenching was further confirmed by our observation that an underneath Ag film produced from sputtering also suppressed the photoluminescence of PbS CQDs spun on top (Figure S5). Both the observations are explainable by the charge transfer between Ag NCs and PbS CQDs. The conduction band (CB) and valence band (VB) edge of our PbS CQDs are located at


dx.doi.org/10.1021/ph500227u | ACS Photonics 2014, 1, 936−943

−3.8 eV and −5.1 eV,[22] and the Fermi energy of Ag NCs stays at −4.3 eV. Upon illumination, photogenerated electrons in PbS CQDs would transfer to Ag NCs, leading to the bleaching of photoluminescence.

On the basis of these observations, we tentatively propose a mechanism for the beneficial effect of Ag NCs brought to the PbS CQD photodetectors (Figure 6). For our PbS CQD/Ag NC composite, Ag NCs were homogeneously distributed inside the bulk film of PbS CQDs. In the dark, because of the difference between the work function of Ag and the Fermi level of PbS CQDs, local band bending would occur between PbS CQDs and Ag NCs, which would work as barriers for hole transport and hence reduce dark current. Ag NCs could also be understood as scattering centers, reducing the hole transport if one assumes band bending is not applicable in these nanocomposites. Under light, PbS CQDs absorb incident light and photoexcited electrons from VB to the CB. Considering its work function position, Ag NCs mainly act as trap states, capturing electrons (minority carrier) from the CB of PbS CQDs. These charges would reside in Ag NCs, and hence the trap lifetime ($\tau$) is prolonged, in analogy with the deep defect in PbS CQDs.[18] As stated previously, the gain ($G$) is defined by the ratio between trap lifetime and the transit time ($\tau_T$): $G = \tau/\tau_T$. Hence a longer trap lifetime would enable holes to circulate more times, leading to higher gain and hence larger photocurrent. This hypothesis is supported by our experimental observation that PbS CQD/Ag NC composite photodetectors had a longer $\tau$ and hence more sluggish photoresponse, as evidenced by the smaller 3 dB frequency. Moreover, a similar photocurrent enhancing effect was reported in PbS CQDs blended with $Bi_2S_3$ NCs. In their binary composites prolonged carrier lifetime over its single component was obtained due to the formation of a nanoscale heterojunction, which can efficiently separate the exciton and increase carrier lifetime.[29]

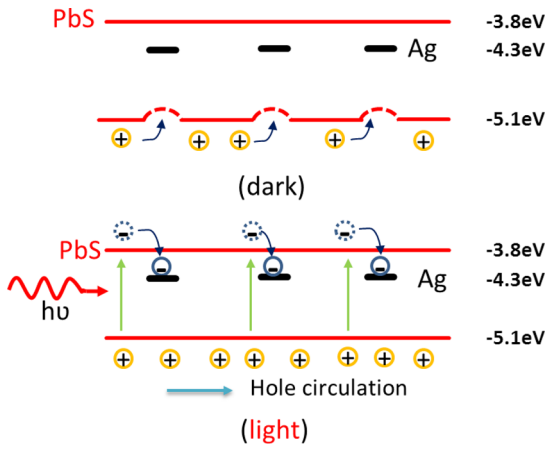


**Figure 6.** Proposed working mechanism. (a) In the dark, Ag NC (black bar) inclusion causes local band bending (red dashed line) and hinders hole transport within the composite film. (b) Under light, photogenerated electrons are trapped by the Ag NCs, leading to more cycles of hole circulation and therefore larger gain and larger photocurrent.

Lightweight and flexible optoelectronics have attracted great research interest because of their many potential applications.[30,31] The present mild device fabrication process and flexibility of the active layer inspired us to further investigate our photodetectors for flexible optoelectronics. The optimized 1% Ag NC composite device was utilized as the active layer, and stone paper was chosen as the substrate because of its

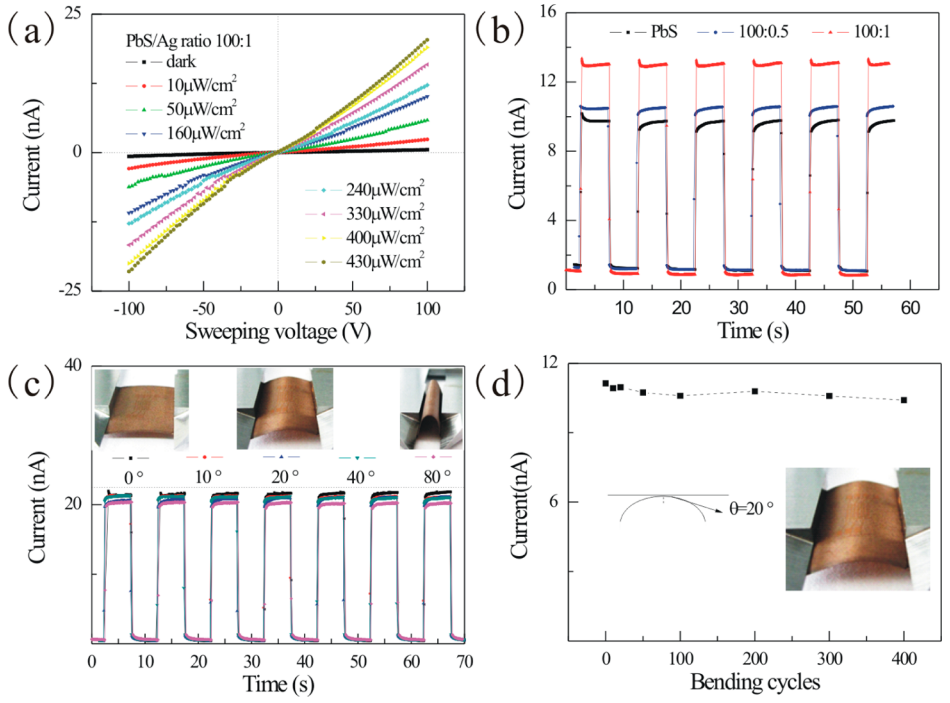


**Figure 7.** Device performance and mechanical flexibility of our PbS CQDs/Ag NCs nanocomposite stone paper photodetector: (a) $I-V$ characteristics of the 1% Ag NC composite device under different light illumination ranging from 10 to 430 $\mu W/cm^2$. (b) $I-t$ curves of composite photodetectors containing different amounts of Ag NCs. (c) Paper-based photodetectors undergoing many cycles of bending and unbending at wide angles (20−80°). The inset shows device photographs of the bending state. (d) Photodetector performances when subjected to multiple cycles of bending at 20°.


dx.doi.org/10.1021/ph500227u | ACS Photonics 2014, 1, 936−943

extremely low cost, high flexibility, smooth surface, and good compatibility with the fabrication process. Figure 7 shows the device performance of our flexible PbS CQD/Ag NC composite photodetector. Figure 7a shows the $I-V$ curves of the photodetector subjected to different intensities of light illumination; the current increased monotonically as the illumination intensified. For the flexible device, Ag NC incorporation also improved photocurrent and reduced dark current simultaneously (Figure 7b), indicating this phenomenon is substrate insensitive. The estimated detectivity reached $1.7 \times 10^{10}$ Jones for the flexible composite device, 54% higher than that of the pure PbS CQD ($1.1 \times 10^{10}$ Jones) analogue. To check their flexibility, we measured device performance under different bending angles (Figure 7c) and after hundreds of bending and releasing cycles (Figure 7d). No discernible degradation was observed when the device was bent between 0° and 80°, and only 10% degradation was observed in device performance when the paper-based photodetector was subjected to 400 cycles of bending and unbending at 20°. Such a robust flexibility, combined with its high detectivity and low-cost manufacturing, suggests the promise of our PbS CQD/Ag NC composite photodetector for potential portable or wearable infrared sensing.

## CONCLUSIONS

In summary, Ag NCs were introduced into PbS CQDs to improve the device performance of solution-processed near-IR photodetectors. As compared with the PbS CQD alone device, the PbS CQD/Ag NC composite photodetector containing 1% (by weight) Ag NCs showed slightly reduced dark current and significantly enhanced photocurrent, leading to the 2.4 times improvement in the estimated device detectivity. A careful mechanism study indicated that leftover oleylamine or $AgNO_3$ from the Ag NC synthesis or in situ formed $Ag_2S$ species during the MPA treatment failed to account for the observation. Instead, we propose that due to their proper work function, Ag NCs could effectively capture photogenerated electrons from the CB of PbS CQDs, extend carrier lifetime, and promote hole circulation and consequently improve photocurrent. We further built a flexible and sensitive PbS CQD/Ag NC composite photodetector, which could represent harsh bending conditions and is suitable for many novel photodetection applications where light weight and mechanical flexibility are required. We believe that the binary NC system may provide some surprising properties that could be utilized as a new strategy to improve the performance of NC-based optoelectronic devices.

## METHODS

**PbS CQD Synthesis.** PbS CQDs were synthesized using a modified method originally developed by Hines.[18] Briefly, 2.25 g of lead(II) oxide, 7.5 mL of oleic acid, and 20 mL of 1-octadecane (ODE) were added in a three-neck flask. This flask was then sealed and heated at 90 °C for 16 h under vigorous stirring and vacuum conditions until the solution became clear and colorless. Then the temperature was elevated to 120 °C, and 0.7 mL of bis(trimethylsilyl)sulfide dissolved in 10 mL of 1-octadecene was quickly injected into the above solution, and the reaction lasted for 5 min. Finally, the heating was turned off and the solution was naturally cooled. Products were precipitated by acetone and redispersed in toluene three times to prepare a 50 mg/mL octane solution ready for device fabrication.

**Ag and $Ag_2S$ NC Synthesis.** Ag NCs were synthesized by the reaction of a 0.18 mol/L $AgNO_3$ and oleylamine solution at 180 °C for 2 h.[19] Products were precipitated by acetone and redispersed in toluene three times to prepare a 50 mg/mL solution ready for device fabrication. The $Ag_2S$ NCs were synthesized by adding 0.05 g of S (dissolved in 5 mL of oleylamine) into a Ag NC solution, then heated at 180 °C for 30 min. Products were treated with acetone and toluene in the same way as Ag NCs. Ag and $Ag_2S$ NCs were weighed, and then a stock solution with known concentration was prepared. The blend solutions were obtained by mixing of the above PbS CQD and Ag NP solutions in varied volume ratios.

**Device Fabrication.** Ceramic chips and stone paper were used as substrates for rigid and flexible IR photodetectors, respectively. Stone paper is made from calcium carbonate mixed with a polyethylene bonding agent. First, the prepatterned interdigitated Au electrodes were deposited on the ceramic chips by thermal evaporation utilizing a shadow mask. The composite film deposition and ligand exchange were carried out inside a fume hood using a layer-by-layer technique. The film was deposited by spin-coating the ready PbS CQD/Ag NC octane solution at 2500 rpm for 30 s. The ligand exchange was then carried out by covering the former film with 3 drops of 10% (v/v in methanol) MPA, which was repeated two times with a 5 s interval. Finally, the film was rinsed three times with 5 drops of methanol each time to remove the residual MPA. The above sequence was repeated another two times to achieve an ~100 nm film thickness. All devices were annealed at 90 °C for 10 min inside a fume hood before characterization.

**Material Characterization.** The prepared materials were characterized by high-resolution transmission electron microscopy (HRTEM, Tecnai $G^2$ 20 U-Twin), X-ray photoelectron spectroscopy (VG Multilab 2000), X-ray diffraction (XRD-7000S/L), and UV−vis absorption spectra (Cary, Lambda 950). Photoluminescence was obtained using a home-built setup using 816 nm laser excitation (Mira 900) and a 0.300 m imaging triple grating monochromator (Acton SP2300).

**Electrical and Optical Measurements.** Photodetector performances were measured using a probe station connected to an Agilent B1500A semiconductor characterization system. The device was further covered with an aluminum cap to provide optical and electromagnetic shielding. Illumination was generated from 850 nm light-emitting diodes controlled by a functional generator (Agilent 33210A). Light intensity was calibrated using a silicon photodetector (Newport 818-UV). The EQE data were obtained upon illumination at different wavelengths obtained from a xenon lamp with a grating monochromator.

## ASSOCIATED CONTENT

### Supporting Information

XRD, XPS, PL, and TEM characterization data of PbS CQD/Ag NC nanocomposites and $Ag_2S$ NCs as well as responsivity versus bias curves of PbS CQD/Ag NC PDs. This material is available free of charge via the Internet at http://pubs.acs.org.

## AUTHOR INFORMATION

### Corresponding Authors

*E-mail (H. Song): songhs-wnlo@mail.hust.edu.cn.
*E-mail (S. Jiang): jsl@mail.hust.edu.cn.
*E-mail (J. Tang): jtang@mail.hust.edu.cn.

### Author Contributions

[§]J. He and K. Qiao contributed equally to this work.

### Notes

The authors declare no competing financial interest.

## ■ ACKNOWLEDGMENTS

This work was financially supported by the seed project of Wuhan National Laboratory for Optoelectronics, by the National Natural Science Foundation of China (61306137, 61274055), by the Independent Innovation Fund of Huazhong University of Science and Technology (HUST: 2013NY002), and by the "National 1000 Young Talents" project. The authors thank the Testing Center of HUST and the Center for Nanoscale Characterization and Devices, Wuhan National Laboratory for Optoelectronics (WNLO), for facility access.

## ■ REFERENCES

(1) Konstantatos, G.; Sargent, E. H. Nanostructured materials for photon detection. *Nat. Nanotechnol.* **2010**, *5*, 391−400.
(2) Hoogland, S.; Sukhovatkin, V.; Shukla, H.; Clifford, J.; Levina, L.; Sargent, E. H. Megahertz-frequency large-area optical modulators at 1.55 μm based on solution-cast colloidal quantum dots. *Opt. Express* **2008**, *16*, 6683−6691.
(3) Kim, S.; Lim, Y. T.; Soltesz, E. G.; De Grand, A. M.; Lee, J.; Nakayama, A.; Parker, J. A.; Mihaljevic, T.; Laurence, R. G.; Dor, D. M.; Cohn, L. H.; Bawendi, M. G.; Frangioni, J. V. Near-infrared fluorescent type II quantum dots for sentinel lymph node mapping. *Nat. Biotechnol.* **2004**, *22*, 93−97.
(4) Ettenberg, M. A little night vision. *Adv. Imaging* **2005**, *20*, 29−32.
(5) Cohen, M. J.; Ettenberg, M. H.; Lange, M. J.; Olsen, G. H. Commercial and industrial applications of indium gallium arsenide near-infrared focal plane arrays. In *AeroSense'99, International Society for Optics and Photonics*; 1999; pp 453−461
(6) Kidder, L.; Levin, I.; Lewis, E. N.; Kleiman, V.; Heilweil, E. Mercury cadmium telluride focal-plane array detection for mid-infrared Fourier-transform spectroscopic imaging. *Opt. Lett.* **1997**, *22*, 742−744.
(7) Cosentino, S.; Liu, P.; Le, S. T.; Lee, S.; Paine, D.; Zaslavsky, A.; Pacifici, D.; Mirabella, S.; Miritello, M.; Crupi, I.; Terrasi, A. High-efficiency silicon-compatible photodetectors based on Ge quantum dots. *Appl. Phys. Lett.* **2011**, *98*, 221107.
(8) Shieh, J. M.; Yu, W. C.; Huang, J. Y.; Wang, C. K.; Dai, B. T.; Jhan, H. Y.; Hsu, C. W.; Kuo, H. C.; Yang, F. L.; Pan, C. L. Near-infrared silicon quantum dots metal-oxide-semiconductor field-effect transistor photodetector. *Appl. Phys. Lett.* **2009**, *94*, 241108.
(9) Konstantatos, G.; Howard, I.; Fischer, A.; Hoogland, S.; Clifford, J.; Klem, E.; Levina, L.; Sargent, E. H. Ultrasensitive solution-cast quantum dot photodetectors. *Nature* **2006**, *442*, 180−183.
(10) Lee, J. S.; Kovalenko, M. V.; Huang, J.; Chung, D. S.; Talapin, D. V. Band-like transport, high electron mobility and high photoconductivity in all-inorganic nanocrystal arrays. *Nat. Nanotechnol.* **2011**, *6*, 348−352.
(11) Pelayo García de Arquer, F.; Beck, F. J.; Bernechea, M. A.; Konstantatos, G. Plasmonic light trapping leads to responsivity increase in colloidal quantum dot photodetectors. *Appl. Phys. Lett.* **2012**, *100*, 043101.
(12) Peng, L.; Tang, J.; Zhu, M. Recent development in colloidal quantum dots photovoltaics. *Front. Optoelectron.* **2012**, *5*, 358−370.
(13) Saran, R.; Nordin, M. N.; Curry, R. J. Facile fabrication of PbS nanocrystal:C-60 fullerite broadband photodetectors with high detectivity. *Adv. Funct. Mater.* **2013**, *23*, 4149−4155.
(14) Konstantatos, G.; Badioli, M.; Gaudreau, L.; Osmond, J.; Bernechea, M.; Garcia de Arquer, F. P.; Gatti, F.; Koppens, F. H. Hybrid graphene-quantum dot phototransistors with ultrahigh gain. *Nat. Nanotechnol.* **2012**, *7*, 363−368.
(15) Konstantatos, G.; Sargent, E. H. Colloidal quantum dot photodetectors. *Infrared Phys. Technol.* **2011**, *54*, 278−282.
(16) Heves, E.; Ozturk, C.; Ozguz, V.; Gurbuz, Y. Solution-based PbS photodiodes, integrable on ROIC, for SWIR detector applications. *IEEE Electron Device Lett.* **2013**, *34*, 662−664.
(17) Lee, S.-S.; Hong, J.-D.; Kim, C. H.; Kim, K.; Koo, J. P.; Lee, K.-B. Layer-by-layer deposited multilayer assemblies of ionene-type polyelectrolytes based on the spin-coating method. *Macromolecules* **2001**, *34*, 5358−5360.
(18) Hines, M. A.; Scholes, G. D. Colloidal PbS nanocrystals with size-tunable near-infrared emission: observation of post-synthesis self-narrowing of the particle size distribution. *Adv. Mater.* **2003**, *15*, 1844−1849.
(19) Shen, C.; Hui, C.; Yang, T.; Xiao, C.; Tian, J.; Bao, L.; Chen, S.; Ding, H.; Gao, H. Monodisperse noble-metal nanoparticles and their surface enhanced Raman scattering properties. *Chem. Mater.* **2008**, *20*, 6939−6944.
(20) Oreels, I.; Lambert, K.; Smeets, D.; De Muynck, D.; Nollet, T.; Martins, J. C.; Vanhaecke, F.; Vantomme, A.; Delerue, C.; Allan, G.; Hens, Z. Size-dependent optical properties of colloidal PbS quantum dots. *ACS Nano* **2009**, *3*, 3023−3030.
(21) Tang, J.; Kemp, K. W.; Hoogland, S.; Jeong, K. S.; Liu, H.; Levina, L.; Furukawa, M.; Wang, X.; Debnath, R.; Cha, D. Colloidal-quantum-dot photovoltaics using atomic-ligand passivation. *Nat. Mater.* **2011**, *10*, 765−771.
(22) Tang, J.; Brzozowski, L.; Barkhouse, D. A.; Wang, X.; Debnath, R.; Wolowiec, R.; Palmiano, E.; Levina, L.; Pattantyus-Abraham, A. G.; Jamakosmanovic, D.; Sargent, E. H. Quantum dot photovoltaics in the extreme quantum confinement regime: the surface-chemical origins of exceptional air- and light-stability. *ACS Nano* **2010**, *4*, 869−878.
(23) Konstantatos, G.; Levina, L.; Tang, J.; Sargent, E. H. Sensitive solution-processed $Bi_2S_3$ nanocrystalline photodetectors. *Nano Lett.* **2008**, *8*, 4002−4006.
(24) Konstantatos, G.; Howard, I.; Fischer, A.; Hoogland, S.; Clifford, J.; Klem, E.; Levina, L.; Sargent, E. H. Ultrasensitive solution-cast quantum dot photodetectors. *Nature* **2006**, *442*, 180−183.
(25) Benzo, P.; Bonafos, C.; Bayle, M.; Carles, R.; Cattaneo, L.; Farcau, C.; Benassayag, G.; Pecassou, B.; Muller, D. Controlled synthesis of buried delta-layers of Ag nanocrystals for near-field plasmonic effects on free surfaces. *J. Appl. Phys.* **2013**, *113*, 193505.
(26) Wen, X.; Xi, Z.; Jiao, X.; Yu, W.; Xue, G.; Zhang, D.; Lu, Y.; Wang, P.; Blair, S.; Ming, H. Plasmonic coupling effect in Ag nanocap-nanohole pairs for surface-enhanced Raman scattering. *Plasmonics* **2013**, *8*, 225−231.
(27) Naumkin, A. V.; Kraut-Vass, A.; Gaarenstroom, S. W.; Powell, C. J. *NIST X-ray Photoelectron Spectroscopy Database NIST*, 2012.
(28) Jiang, P.; Zhu, C.-N.; Zhang, Z.-L.; Tian, Z.-Q.; Pang, D.-W. Water-soluble $Ag_2S$ quantum dots for near-infrared fluorescence imaging in vivo. *Biomaterials* **2012**, *33*, 5130−5135.
(29) Rath, A. K.; Bernechea, M.; Martinez, L.; de Arquer, F. P. G.; Osmond, J.; Konstantatos, G. Solution-processed inorganic bulk nano-heterojunctions and their application to solar cells. *Nat. Photonics* **2012**, *6*, 529−534.
(30) Tan, Z.; Xu, J.; Zhang, C.; Zhu, T.; Zhang, F.; Hedrick, B.; Pickering, S.; Wu, J.; Su, H.; Gao, S. Colloidal nanocrystal-based light-emitting diodes fabricated on plastic toward flexible quantum dot optoelectronics. *J. Appl. Phys.* **2009**, *105*, 034312.
(31) Lee, C. H.; Kim, Y. J.; Hong, Y. J.; Jeon, S. R.; Bae, S.; Hong, B. H.; Yi, G. C. Flexible inorganic nanostructure light-emitting diodes fabricated on graphene films. *Adv. Mater.* **2011**, *23*, 4614−4619.